Nanoarchitectonics
http://ojs.wiserpub.com/index.php/NAT/

UNIVERSAL WISER PUBLISHER

Research Article

Influence of Annealing Temperature on the Properties of SILAR Deposited CdSe/ZnSe Superlattice Thin Films for Optoelectronic Applications

C. I. Elekalachi[1*], I. A. Ezenwa[1], A. N. Okereke[1], N. L. Okoli[2], A. N. Nwori[1]

[1]Department of Industrial Physics, Faculty of Physical Science, Chukwuemeka Odumegwu Ojukwu University, Uli, Anambra State, Nigeria
[2]Department of Physics and Electronics, Faculty of Natural and Applied Sciences, Legacy University Okija, Anambra State, Nigeria
E-mail: ci.elekalachi@coou.edu.ng

Received: 25 June 2022; **Revised:** 16 August 2022; **Accepted:** 20 August 2022

Abstract: In this work, superlattice thin films of CdSe/ZnSe were fabricated on a non-conductive glass substrate using the successive ionic layer adsorption reaction (SILAR) method to investigate their properties for possible optoelectronic applications. The SILAR process involved a total cycle time of 100 seconds for a complete SILAR cycle with a total of 12 cycles made by depositing alternative layers of CdSe and ZnSe. The deposited thin films were annealed at different temperatures and characterized to determine their optical, elemental, morphological and structural properties using UV-Vis spectroscopy, Scanning electron microscope (SEM)/energy dispersive x-ray spectroscope (EDS) and x-ray diffraction techniques (XRD). The results of the characterizations revealed that optical properties of the films such as absorbance, reflectance, refractive index and extinction coefficient are low but increased as the annealing temperature increases. The bandgap energy was found to decrease from 2.50 eV-1.90 eV for as-deposited film and those annealed between 373 K and 523 K. Film thickness was found to range from 130.169 nm to 254.441 nm. The EDS results showed that the target elements such as Cd, Zn, Se and other elements traceable to the nature of substrate used were found to be present in the deposited thin film samples. The results of the XRD showed that the thin films are polycrystalline and the diffraction peaks are influenced by annealing of the sample at a higher temperature such as 523 K. The crystal parameters such as crystallite size, dislocation density and micro-strain of the film at 523 K were found to be 5.546 nm, 3.25×10^{16} l/m^2 and 1.13×10^{-2}. The SEM results showed that the CdSe/ZnSe superlattice films were composed of tiny nanoparticles of different dimensions and sizes with hollow which increased as the annealing temperature increased from 432 K to 523 K. Possible applications of the deposited superlattice thin films in solar cells and optoelectronic devices were established by virtue of their bandgap energy and other properties.

Keywords: CdSe/ZnSe superlattice, optoelectronics, bandgap, chalcogenide, absorbance, solar cells

1. Introduction

The potential for many applications in the fields of electronics and optoelectronic devices exhibited by the group II-VI chalcogenide semiconductor materials like CdSe, ZnSe and others have led many researchers to further investigate the applications of the materials at their nanostructure levels. Research has shown that metal chalcogenides in the case

DOI: https://doi.org/10.37256/nat.4120231650

of CdSe and ZnSe semiconductors are good materials for applications in photovoltaic solar cells, photo-detectors, light amplifiers, lasers, gas sensors, large screen liquid crystal display, photoluminescence response, light-emitting diodes, photo-catalysis, and optically sensitive devices applications ([1-3]. These applications have been attributed to the high absorption coefficient and optimum bandgap energy the materials possessed for efficient light absorption and consequent conversion of the light energy to electrical energy [4].

CdSe is an n-type semiconductor material of the group II-VI chalcogenide family which has a direct bandgap energy of ~1.80 eV for wurtzite crystal phase and ~1.71 eV for zinc blende crystal phase structures. This singular property has been tipped to position the CdSe as excellent material for optoelectronic applications including biomedical imaging as human tissue is permeable to near infra-red light and the bandgap favors absorption in the visible and near-infrared range [5-7]. On the other hand, ZnSe is an important n-type semiconductor but has a direct bandgap energy of 2.70 eV [8-9] and has been known to be a highly photosensitive semiconductor as its bandgap ranges in the visible region of the electromagnetic spectrum [10]. The quest by the researchers to further study the characteristics of these semiconductor materials at their atomic and nanostructure levels has led to the manipulations of the materials through many processes such as doping with different elements and fabrications of layers of these materials on top of one another [11-12].

To this effect, many deposition methods have been used to fabricate different thin film structures of CdSe and ZnSe to study their basic properties for applications. [13-14] used the electrodeposition method to fabricate thin films of CdSe/ZnSe and stated that the superlattice films of CdSe/ZnSe are good materials to be used for antireflection coatings. The thin films of $Zn_{1-x}Mg_xS$ deposited using RF magnetron co-sputtering technique by [15] are influenced by Mg ion doping and tuned the bandgap energy to values that range from 4.39 eV to 3.25 eV which was found to be useful for window layers of thin film photovoltaic devices. Yttrium doped CdSe thin film deposited using the spray pyrolysis method has been reported by [16] that showed various influences of Yttrium on different properties of the CdSe films. The results showed that the influence of Y: CdSe and annealing temperatures positioned the films as a better material for use in photovoltaic, electronic, and optoelectronics applications. The effect of Mn-doped ZnSe passivation layer on the performance of CdS/CdSe quantum dot sensitized solar cells fabricated using the SILAR method reported by [17] showed that Mn-doped ZnSe as a passivation layer on the surface of TiO_2/CdS/CdSe co-sensitized solar cells can effectively improve the power conversion efficiency (PCE) of solar cells by 9% compared to a device without manganese doping. [18] used electrodeposition method to fabricate thin films of CdSe and (Fe, Mn) doped CdSe and reported that the undoped CdSe, Fe-CdSe and Mn-CdSe thin films can be used as solar cell and photoelectrochemical (PEC) cell materials. The effect of different selective ligands such as thiols 3-mercaptopropionic acid (MPA), thioglycolic acid (TGA), and L-glutathione (GSH) on the properties of ZnSe and $Zn_xCd_{1-x}Se$ QDs deposited using water-based route to ligand-selective synthesis have been reported by [19]. Their results showed that the ligands have different effects on the optical, structural and morphological properties of the materials. Other methods that can separate QDs from reaction constituents and link them with other materials to utilize them for biological labels, biosensors, light-emitting diodes, lasers devices applications were suggested by the authors. [20] used the atomic layer deposition method to fabricate ZnSe/CdSe superlattice nanowires and concluded that the nanowires are single crystal but comprised of alternating layers of lattice plane (111) oriented ZnSe and CdSe which were oriented at 60° to each other.

In this work, superlattice thin films of CdSe/ZnSe were fabricated using the SILAR method. Deposited superlattice films were annealed at a varying temperature ranges from 373 K to 523 K. Effects of annealing temperature on the optical, morphological and compositional properties of the deposited superlattice thin films were determined. Structural analysis was used to confirm the formation of CdSe and ZnSe thin films.

2. Materials and method

2.1 *Materials*

The reagents used for the synthesis of the superlattice thin films of the CdSe/ZnSe are cadmium (II) chloride hemi(pentahydrate) (Kermel), zinc (II) acetate dehydrate (Qualikems), selenium (IV) oxide (JT Baker Chemical Company), sodium borohydride (Kermel) and sodium hydrogen selenide. All the chemicals used for this experiment were of analytical grade and were used without further purification. Sodium hydrogen selenide was prepared by reacting

selenium (IV) oxide with sodium borohydride at room temperature. Freshly prepared sodium hydrogen selenide was used for the experiment because it decomposes in moist air with the formation of polyselenides and precipitation of Se.

2.2 *Experimental details*

The reagents are of analytical grade and were used without further purification. Preferred molar solutions of the reagents were prepared using the general equation (1) to determine their reacting mass.

$$Reacting\ Mass = \frac{molarity \times molar\ mass \times volume}{1000} \quad (1)$$

0.20 M of cadmium (II) chloride hemi(pentahydrate) and 0.20 M of zinc acetate dihydrate were prepared by dissolving 22.84 g and 21.95 g of the compounds respectively in 500 mL of distilled water. These prepared solutions of the compounds served as precursors for Cd^{2+} and Zn^{2+}. Sodium hydrogen selenide was used as the precursor for selenium ion and was prepared by a reaction between sodium borohydride and selenium (IV) oxide at room temperature. The reaction involves the mixture of 40 mL of 0.05 M of selenium (IV) oxide with 40 mL of 0.03 M of sodium borohydride. The solution was freshly prepared before its use as it is relatively unstable. Before the deposition, the substrates were soaked in trioxonitrate (V) acid for 48 hours, washed with detergent and rinsed with distilled water. The substrates were subjected to ultrasonic cleaning with a solution of acetone in water of volume ratio (3:1) at 50 °C for 30 minutes. The degreased substrates were rinsed 3 times with distilled water and finally dried in an electric oven at 60 °C for 15 minutes.

The superlattice thin films of CdSe/ZnSe were synthesized at room temperature using the successive ion layer adsorption reaction (SILAR) method. The temperature of the laboratory during deposition was found to be 27 °C (300 K). Four beakers were used with the first beaker labeled A containing cationic precursors ($CdCl_2$ or Zn(ace)), the second beaker labeled B containing ionic exchange medium (distilled water), beaker C containing anionic precursor (NaHSe) while the last beaker labeled D contains ionic exchange medium (distilled water). The SILAR process involved a total cycle time of 100 seconds for one complete cycle and included the following four steps as demonstrated in Figure 1.

Immersion of cleaned substrates in first reaction beaker (A) containing Cd^{2+} precursor solution for 40 s to absorb Cd^{2+} on the surface of the substrate.

These substrates were rinsed in high purity distilled water for 10 s to remove excess Cd^{2+} that are loosely adherent to the glass substrates (achieved in the previous step).

The substrates were then immersed in the anionic precursor solution of freshly prepared NaHSe for another 40 s. The selenide (Se^{2-}) ions reacted with the absorbed Cd^{2+} on the active center of the substrates to form metal selenide films.

Again, the substrates were rinsed in distilled water for 10 s to remove loosely bound ions present on the substrates and unreacted cations and anions and this completed one cycle.

The above process was repeated for six alternating layers of both CdSe and ZnSe and which completed the formation of superlattice thin film layers of CdSe/ZnSe. Figure 1 shows the experimental step-up for SILAR deposition of CdSe and ZnSe thin film layers. The alternating layer deposition implied the deposition of a single layer of CdSe thin film followed by deposition of a single layer of ZnSe thin film. This alternating procedure was repeated on the same substrates five more times for each binary selenide. Five samples of the CdSe/ZnSe superlattice thin films were fabricated. One of the deposited thin films was left unannealed (as-deposited) while four others were annealed at different temperatures as illustrated in Table 1. The result is the formation of CdSe/ZnSe superlattice thin film as shown in Figure 2.

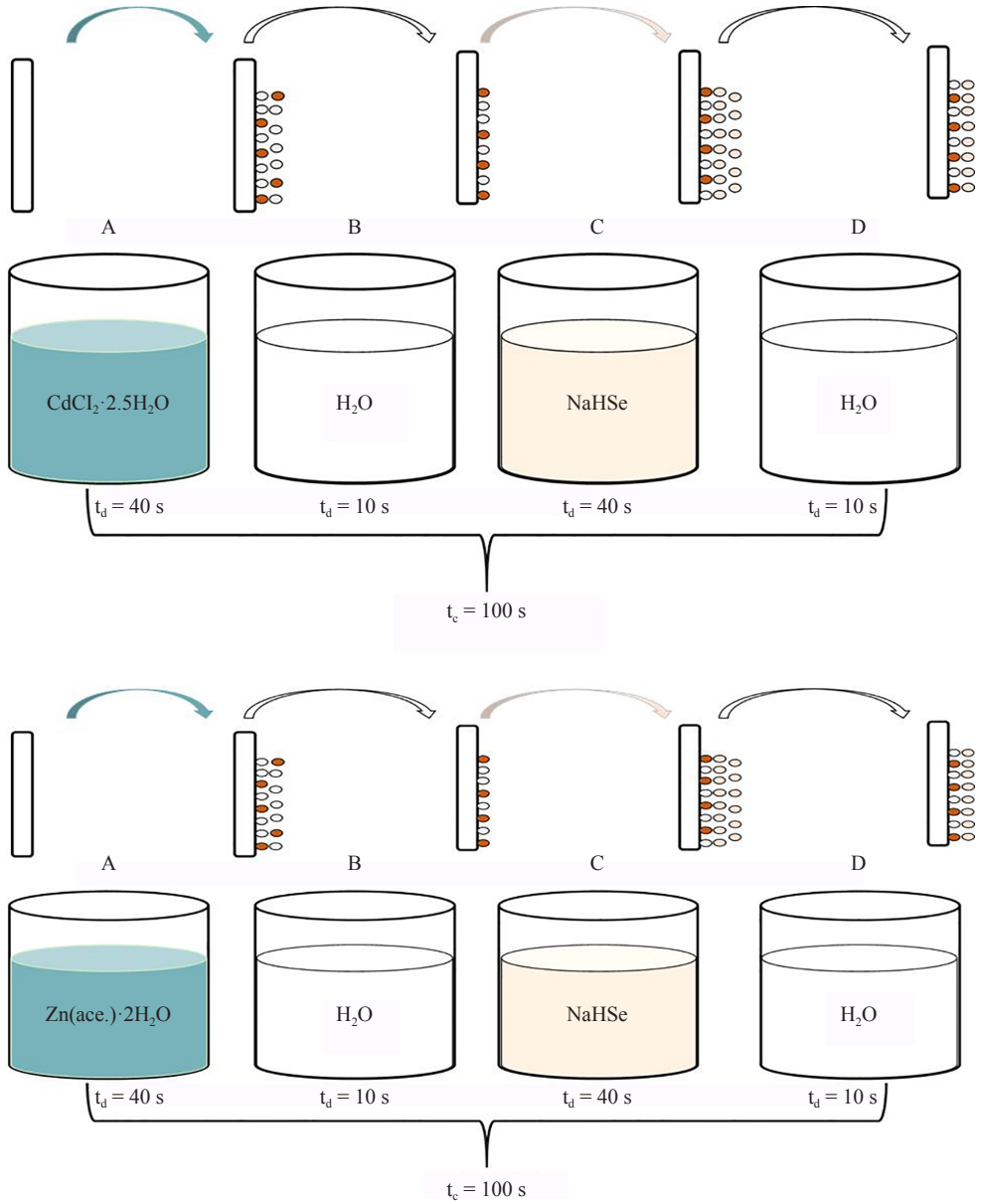

Figure 1. Experimental set-up for SILAR deposition of CdSe/ZnSe superlattice thin films

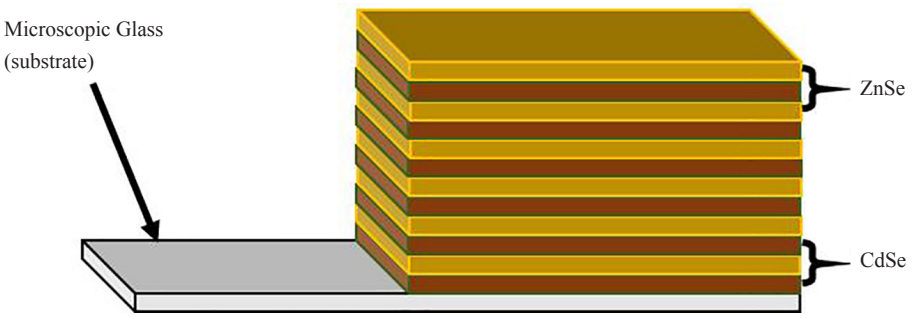

Figure 2. Schematic description of formed superlattice structure for CdSe/ZnSe thin films

Table 1. Optimization of annealing temperature for CdSe/ZnSe thin films

Sample name	Annealed temp. for 60 minutes (K)
CdSe/ZnSe@300K	300
CdSe/ZnSe@373K	373
CdSe/ZnSe@423K	423
CdSe/ZnSe@473K	473
CdSe/ZnSe@523K	523

2.3 *Thin film characterization*

Optical and electrical properties were evaluated using UV-VIS spectrophotometer (model: 756S UV-VIS). Film thickness was carried out using the gravimetric method. Differences in the weights of the substrates before and after deposition were measured using a precision analytical digital balance with a sensitivity of 0.0001 g (0.1 mg). Morphological analysis of the film was done using scanning electron microscope (MIRA TESCAN SEM). Structural analyses of the thin films were studied using the X-ray diffraction (XRD) machine (Buker D8 high resolution diffractometer).

3. Results and discussions

3.1 *Optical properties*

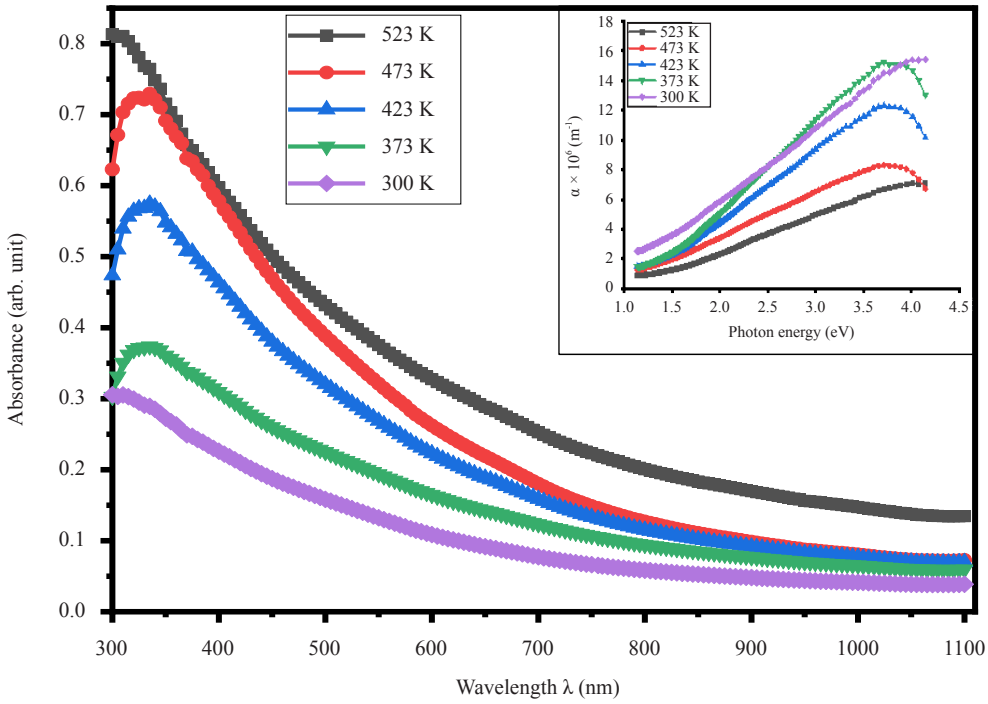

Figure 3. Graph of absorbance against wavelength for CdSe/ZnSe thin films (effect of annealing)

Figure 3 is the graph of absorbance against wavelength and absorption coefficient plotted against photon energy for the fabricated superlattice thin films of CdSe/ZnSe annealed at different temperatures to determine the effect of heat treatment on their optical properties. The Figure showed that the characteristic peak in the absorbance occurred at the UV-A band and increases with an increase in the annealing temperature. The films 523 K and 300 K have the highest and lowest values of absorbance respectively in the UV, VIS and NIR regions. The absorbance however decreases with an increase in wavelength in the VIS and NIR regions suggesting lower values in the NIR region. This increase in absorbance is complemented by a corresponding increase in film thickness. Absorption coefficient values of the thin films were found to possess similar variation as absorbance values. Absorption coefficient values of the films were found to range from $8.96 \times 10^5\ m^{-1}$ to $15.42 \times 10^6\ m^{-1}$. The increase in the absorbance of the films as a result of annealing temperature positions them to be used as absorber materials for photovoltaic applications.

The transmittance of the deposited thin films of CdSe/ZnSe was evaluated using equation (2) which gives the relationship between absorbance and transmittance as given by [21].

$$T = 10^{-A} \tag{2}$$

Where A is the measured absorbance of the films from the spectrophotometer machine.

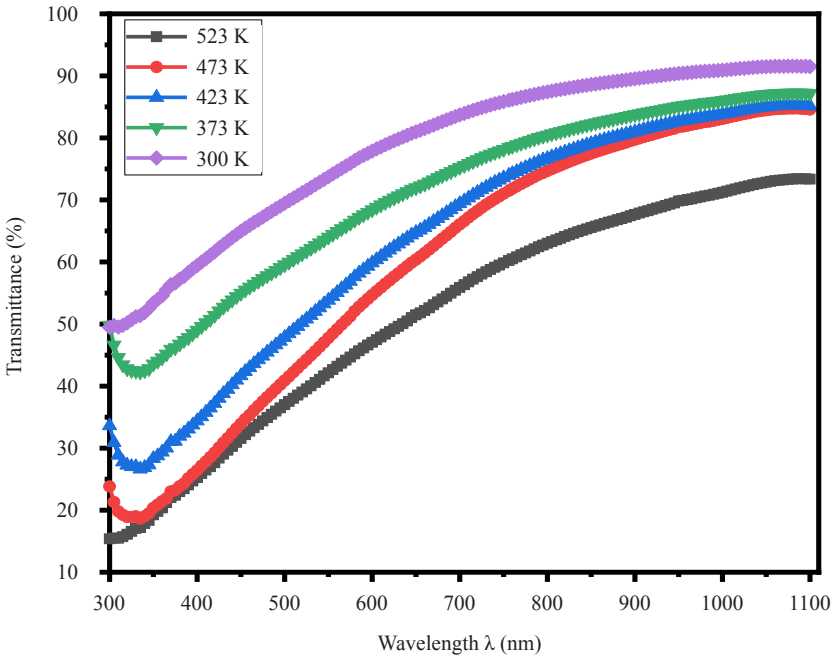

Figure 4. Graph of Transmittance (%) against wavelength for CdSe/ZnSe thin films (effect of annealing)

In Figure 4, the graph of percentage transmittance against wavelength for the fabricated thin films annealed at different temperatures is presented. The Figure showed that the films have high transmittance but decrease with an increase in annealing temperature. The transmittance of the films however increases with an increase in wavelength throughout the VIS and NIR regions of the electromagnetic spectrum (EMS). The film 300 K has the highest transmittance in the range of 50-90 % while the film 523 K has the lowest transmittance in the range of 15-70 % in the VIS and NIR regions. This high transmittance in the NIR region makes the films good materials to be approximated be used as a cold mirror when optimized.

The reflectance (R) of the deposited films was calculated using the law of conservation of radiant energy relating to absorbance, transmittance and reflectance as shown in equation (3) according to [22-24].

$$A + T + R = 1. \tag{3}$$

Where A and T are absorbance and transmittance of the films respectively.

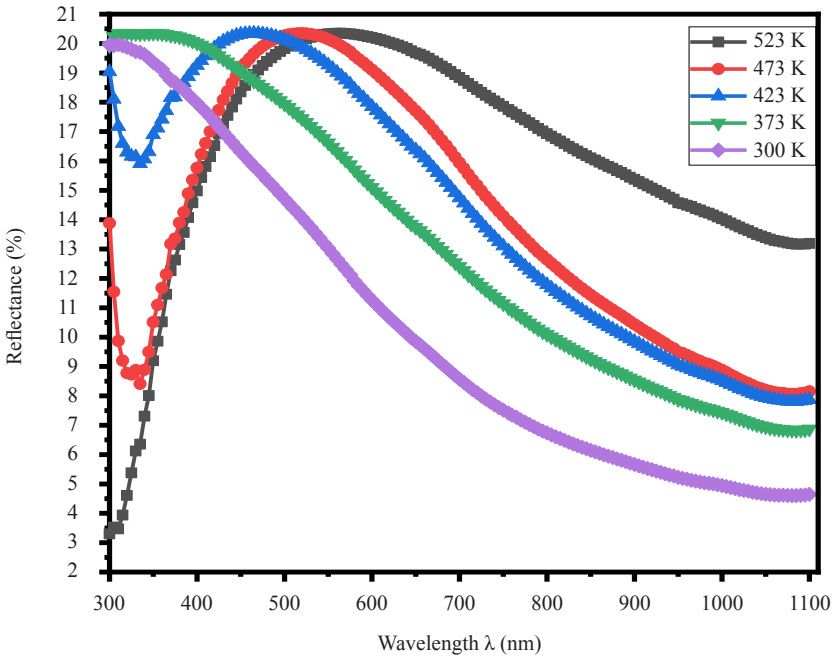

Figure 5. Graph of Reflectance (%) against wavelength for CdSe/ZnSe thin films (effect of annealing)

The graph of reflectance against wavelength for the fabricated thin films CdSe/ZnSe annealed at different temperatures is presented in Figure 5. The graph showed that the reflectance of the films is low with maximum reflectance of 20 %. The characteristic peaks are shifted towards the VIS region as a result of an increase in annealing temperature. The graph also showed that the reflectance decreases with a wavelength in the remaining parts of VIS and NIR regions of EMS.

Refractive index of the films was evaluated using the equation (4) as given by [25-28].

$$\eta = \frac{1+R}{1-R} + \sqrt{\frac{4R}{(1-R)^2} - k^2} \tag{4}$$

Where R is the reflectance of the films.

The plot of refractive index of the fabricated thin films at different annealing temperatures is displayed in Figure 6. The Figure showed that the refractive index of the films is high with the characteristic peaks value of 2.6 being shifted towards the VIS region due to annealing of the samples. The refractive increased with an increase in the annealing temperature but decreases with a wavelength in the VIS and NIR regions. The high refractive index values of the films position them for optical waveguide applications.

The extinction coefficient (k) of the deposited thin films was calculated using equation (5) as given by [29-30].

$$k = \frac{\alpha\lambda}{4\pi}. \tag{5}$$

Where *k* is called the extinction coefficient or attenuation constant of the film.

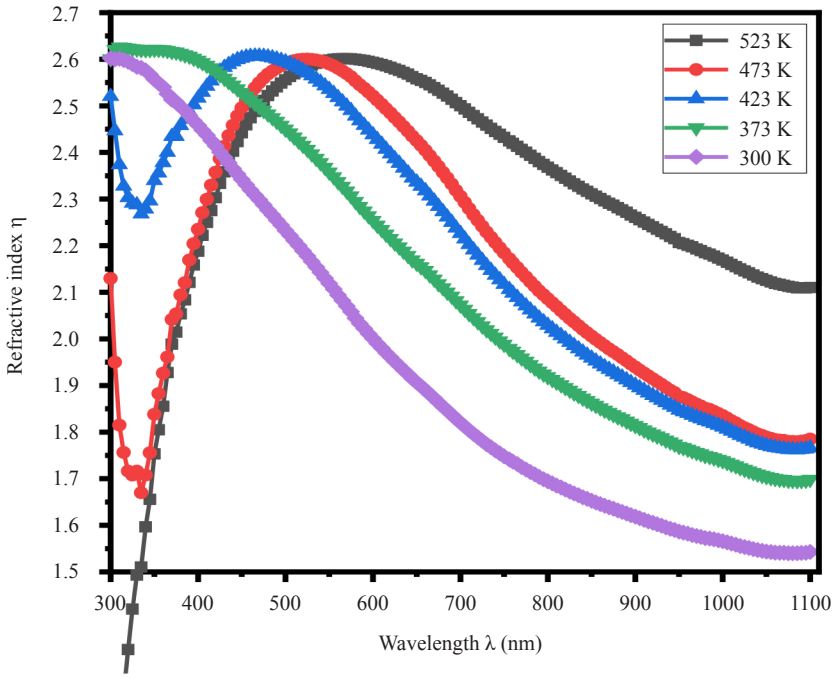

Figure 6. Graph of Refractive index against wavelength for CdSe/ZnSe thin film (effect of annealing)

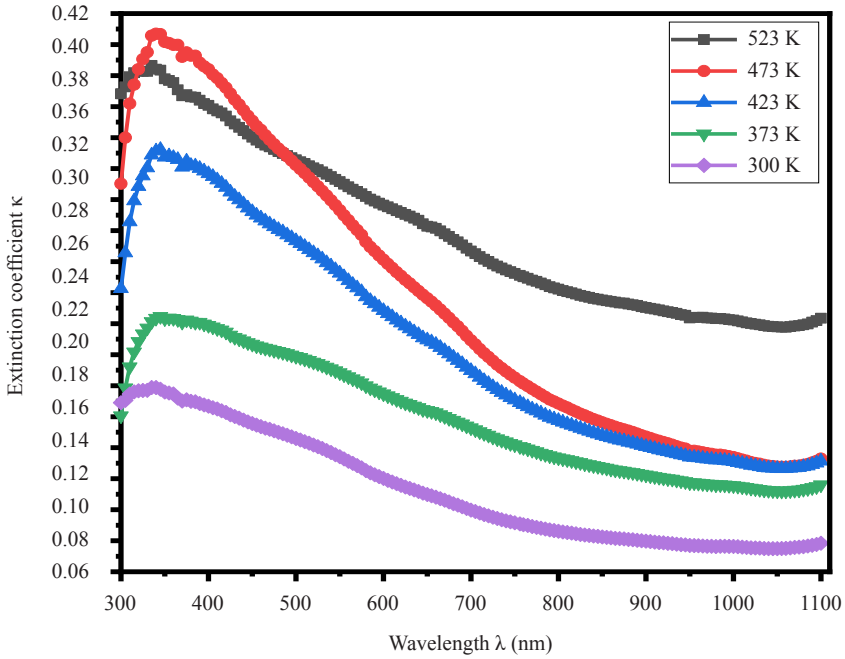

Figure 7. Graph of Extinction coefficient against wavelength for CdSe/ZnSe thin film (effect of annealing)

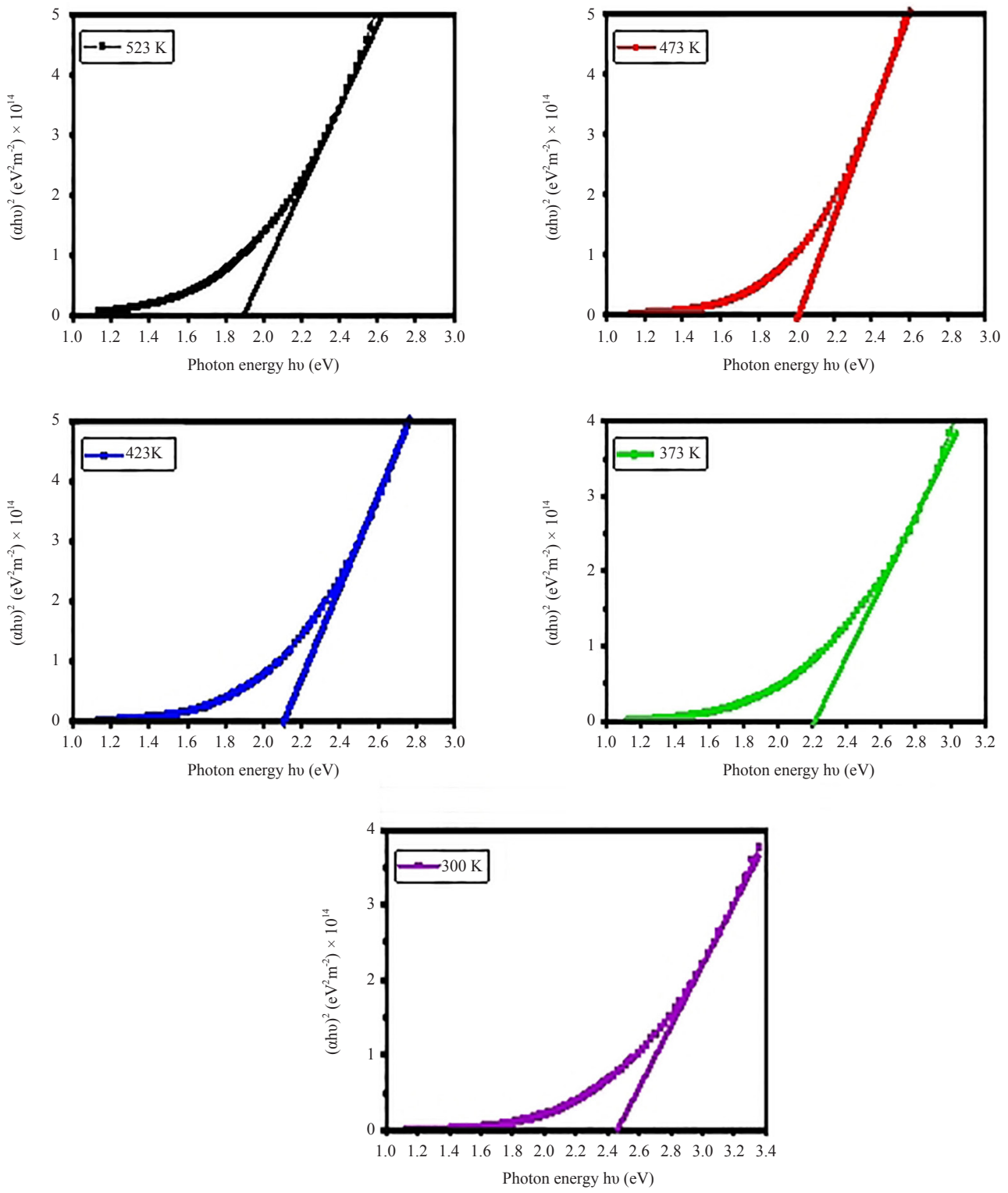

Figure 8. Plots of $(\alpha h\upsilon)^2$ against photon energy for CdSe/ZnSe thin films (effect of annealing)

Figure 7 is the graph of extinction coefficient of the films plotted against wavelength. Extinction coefficient is a measure of the rate at which light energy is retained or lost in the materials. The graph showed that the films have low

values of extinction coefficient but increased with an increase in annealing temperature within VIS and NIR regions. The graph also showed that the extinction coefficient of the films decreased as wavelength increased in the VIS and NIR regions of EMS. This decrease in extinction coefficient as wavelength increases shows that some fraction of radiation was lost due to scattering and absorption of EMS within the films. High extinction coefficient between wavelength of 315 nm and 485 nm observed in superlattice thin film annealed at 473 K was due to absorption peak at 335 nm. The low extinction coefficient exhibited by films makes them suitable materials for many optoelectronic applications.

The optical bandgap energy of the superlattice thin films was calculated using the equation (6) according to [31-32].

$$\alpha hv = A(hv - E_g)^n \tag{6}$$

Where h is Planck's constant and n = 1/2, if the transitions between the upper part of the valence band and the lower part of the conduction band are allowed by the selection rules and n = 3/2, if the transition is forbidden, υ is the frequency, A is constants and E_g is the optical bandgap energy. The plots of $(\alpha h\upsilon)^2$ against photon energy for the CdSe/ZnSe thin films annealed at different temperatures are displayed in Figure 8 in order to determine the energy band gap of the films. The plots showed that the films have wide band gap values but decrease with an increase in the annealing temperature. The band gaps of the films obtained by extrapolating on the photon energy axis at the absorption edged where $(\alpha h\upsilon)^2 = 0$ are 2.50 eV, 2.20 eV, 2.15 eV, 2.00 eV and 1.90 eV for the films annealed at 300 K, 373 K, 423 K, 473 K and 523 K respectively. This noticeable red shift may be a result of increase in crystallite size as rightly revealed by XRD results. This resulted in decrease in defect concentration as well as reduced the strain in the film. This decrease is due to quantum confinement effect within the thin films. A similar red shift in bandgap due to increase in annealing temperature was observed by [33-35]. These bandgap energy values are within the range of bandgap energy reported by [36] for CdSe:Zn thin films deposited using electron beam evaporation method. These values are in the range of energies for photons in the solar spectrum for solar cell and LED applications.

3.2 *Film thickness properties*

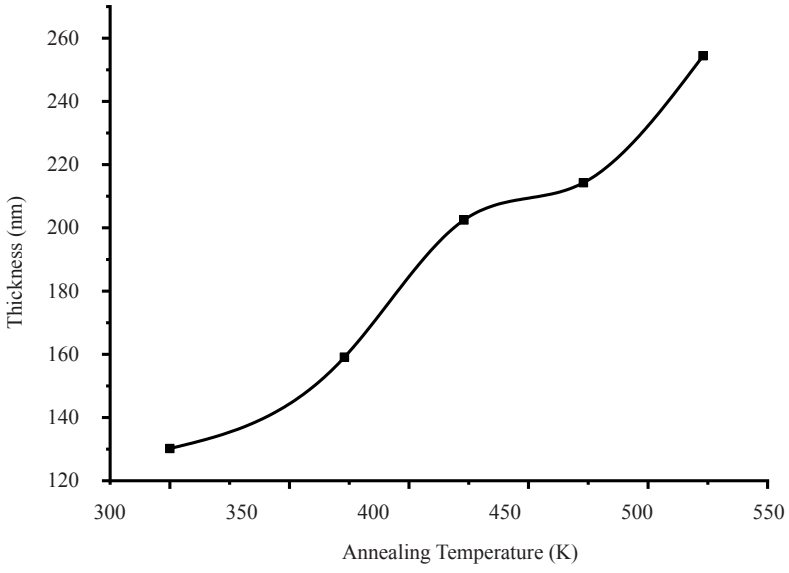

Figure 9. Film thickness plotted against annealing temperature for SILAR deposited cadmium selenide/zinc selenide superlattice

The thicknesses (t) of the deposited thin films were evaluated using the gravimetric method given by [37-40]. Equation (7) gives the relationship between mass difference of the substrate, density of the thin film compound and surface area of the deposited thin film.

$$t = \frac{\Delta m}{\rho A} \tag{7}$$

where Δm is the difference in mass. A is the surface area of the deposited film and ρ is the bulk density of the material film. The masses of the deposited films were obtained by finding the difference in mass between the mass of the glass substrate and the film after deposition and the mass of glass substrate before deposition.

Table 2. Variation of Film thickness, energy bandgap with Annealing Temperature for CdSe/ZnSe Superlattice thin films

Annealing Temp. (K)	Energy Bandgap (eV)	Thickness (nm)
300	2.50	130.167
373	2.20	159.093
423	2.15	202.482
473	2.00	214.266
523	1.90	254.441

Table 2 shows the variation of film thickness with annealing temperature for SILAR deposited CdSe/ZnSe superlattice thin films. Figure 9 shows the plot of variation of film thickness with annealing temperature. For CdSe/ZnSe superlattice thin films annealed at different temperatures from 373 K to 523 K, values of film thickness were found to increase from 159.093 nm to 254.441 nm while as-deposited CdSe/ZnSe superlattice thin film was found to possess the least thickness of 130.167 nm. This result showed that the thickness of the superlattice film is been affected by the change in annealing temperature from 373 K to 523 K. Similar results of increase in film thickness due to an increase in annealing temperature were reported by [41-43]. The increase in film thickness could be due to quantum confinement effect and also due to change in barrier height owing to change in grain size of polycrystalline CdSe/ZnSe thin film as confirmed by XRD results [44].

3.3 *Compositional properties*

Figure 10 showed the EDS graphs of SILAR deposited CdSe/ZnSe thin films, as-deposited (300 K) and those annealed at 423 K and 523 K. Atomic percentages of the elements present in the deposited thin films were presented along with the EDS spectra. The EDS spectra confirmed the presence of Cadmium (Cd), Zinc (Zn), selenium (Se) and other elements such as carbon (C), oxygen (O), sodium (Na), Magnesium (Mg), silicon (Si), copper (Cu), calcium (Ca) and Chlorine (Cl). These other elements may be due to the composition of the microscopic glass used as a substrate for the deposition. As-deposited (300 K) CdSe/ZnSe thin film contained 17.67% of Zn, 21.10% of Cd and 22.17% of Se. After annealing at 423 K and 523 K, Zn content was found to decrease to 10.06%, Cd content was found to increase from 21.10% at 300 K to 27.61% and 27.08% for 423 K and 523 K respectively while Se content increased from 22.17% to 33.64% at 423 K before decreasing to 28.01% at 523 K. These results revealed the dependency of compositional properties of CdSe/ZnSe superlattice thin films on annealing temperature. Thin film relatively rich in selenium was obtained at 423 K and 523 K.

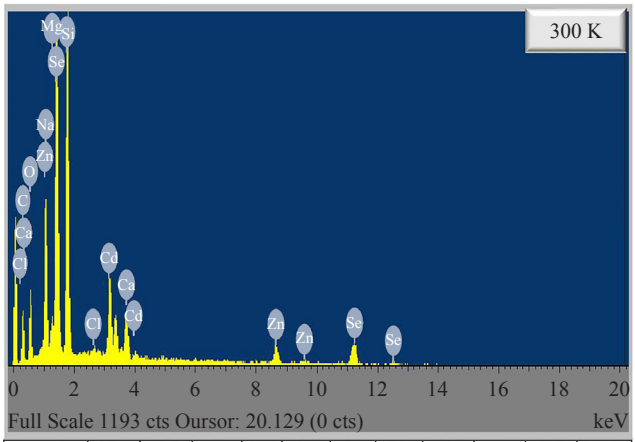

Elements	C	O	Na	Mg	Si	Cl	Ca	Zn	Se	Cd	Total
Atomic (%)	10.63	11.18	4.58	0.6	9.00	0.35	2.75	17.64	22.17	21.10	100

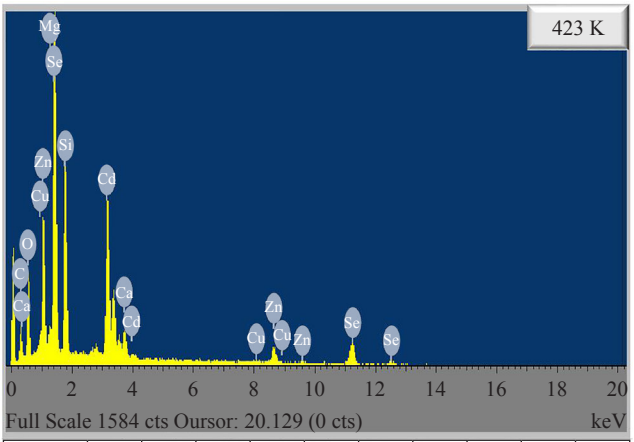

Elements	C	O	Mg	Si	Ca	Cu	Zn	Se	Cd	Total
Atomic (%)	8.03	9.67	0.5	5.1	1.41	0.50	12.54	34.64	27.61	100

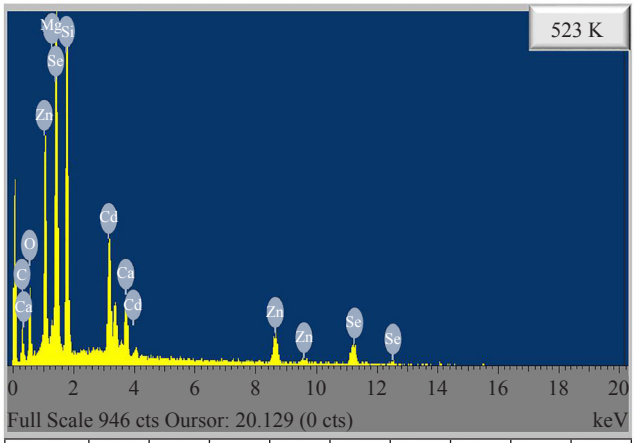

Elements	C	O	Mg	Si	Ca	Zn	Se	Cd	Total
Atomic (%)	11.63	15.05	1.23	5.02	1.93	10.06	28.01	27.08	100

Figure 10. EDS spectra of SILAR deposited CdSe/ZnSe thin films at 300 K, annealed at 423 K and 523 K

3.4 *Structural properties*

Figure 11 shows the x-ray diffraction patterns of as-deposited CdSe/ZnSe thin film at room temperature and CdSe/ZnSe thin film annealed at 523 K. The X-ray diffractogram of as-deposited CdSe/ZnSe thin films showed a weak peak that could not be assigned to any phase of either CdSe or ZnSe which confirmed that the as-deposited CdSe/ZnSe thin film has amorphous structure. Diffractogram of SILAR deposited CdSe/ZnSe thin film annealed at 523 K showed peaks corresponding to hexagonal phases of cadmium selenide and zinc selenide respectively. Four peaks corresponded to standard Powder Diffraction File (PDF) card number 01-077-2307 for hexagonal CdSe. Three peaks corresponded to the peaks in the standard Powder Diffraction File (PDF) card number 01-080-0008 for ZnSe [45-46]. The diffraction spectra showed an increase in intensity at annealing temperature of 523 K. Also, the result showed that the deposited thin films are polycrystalline in nature. No diffraction peaks corresponding to other phases of either ZnSe, CdSe or ternary derivatives of the elements were observed. Table 3 shows the structural parameters of CdSe/ZnSe thin films annealed at 523 K. Slight peak shift was observed between the standard and observed peak values as shown in Figure 3. This shows that there is change in the lattice structure of the films at a high annealing temperature of 523 K.

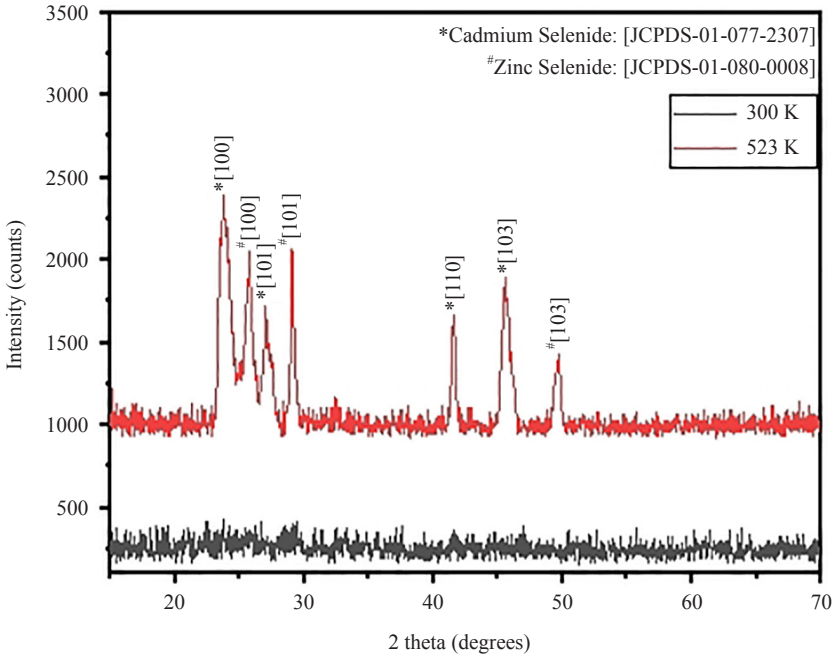

Figure 11. XRD pattern of cadmium selenide/zinc selenide (CdSe/ZnSe) thin films, as-deposited and annealed at 523 K

Table 3. Crystal structural properties of CdSe/ZnSe thin films

Observed		Standard		[hkl]	FWHM	4sinθ	βcosθ
2θ (°)	d-spacing (Å)	2θ (°)	d-spacing (Å)		(°)		
23.934*	3.715	23.882	3.723	100	1.008	0.829	0.017
25.746#	3.457	25.867	3.441	100	0.884	0.891	0.015
27.206*	3.275	27.092	3.288	101	0.815	0.941	0.014
29.154#	3.061	29.335	3.042	101	0.371	1.007	0.006
41.624*	2.168	41.999	2.150	110	0.364	1.421	0.006
45.678*	1.985	45.810	1.979	103	0.747	1.553	0.012
49.650#	1.835	49.648	1.835	103	0.525	1.679	0.008

Williamson-Hall method was used to determine the structural parameters of the deposited thin films. The Bragg peak breadth is a combination of both instrument and sample dependent effects. To take care of these aberrations, it is needed to assemble a diffraction pattern from the line broadening of standard material such as silicon to determine the instrumental broadening. The instrument corrected broadening β_D corresponding to the diffraction peaks is given by [47-50] as

$$\beta_D^2 = [\beta_{measure}^2 - \beta_{instrument}^2] \quad (8)$$

According to Debye-Scherrer's formula for determination of crystallite size as given by [51-53] in equation (9),

$$D = \frac{k\lambda}{\beta_D \cos\theta} \Rightarrow \cos\theta = \frac{k\lambda}{D}\left(\frac{1}{\beta_D}\right) \tag{9}$$

β_D is expressed as

$$\beta_D = \frac{k\lambda}{D\cos\theta} \tag{10}$$

While the crystal imperfection and distortion of strain-induced peak broadening is related by

$$\varepsilon = \frac{\beta_s}{\tan\theta} \tag{11}$$

Where D is the crystallite size (grain size), λ is the wavelength of the x-ray radiation, θ is the angle of diffraction. The extraordinary property of equation (9) is its dependency on the diffraction angle (θ). Depending on different θ positions, the separation of size and strain broadening analysis is done using Williamson-Hall method. When equations (9), (10) and (11) are combined, we have that

$$\beta_{hkl} = \beta_s + \beta_D$$

$$\beta_{hkl} = \left(\frac{k\lambda}{D\cos\theta}\right) + 4\varepsilon\tan\theta$$

$$\beta_{hkl}\cos\theta = \left(\frac{k\lambda}{D}\right) + 4\varepsilon\sin\theta$$

$$\beta\cos\theta = \left(\frac{0.9\lambda}{D}\right) + 4\varepsilon\sin\theta \tag{12}$$

Where β is the full width half maximum (FWHM), ε is the microstrain. A plot of β against $4\sin\theta$ which is regarded as Hall-Williamson plot gives the slope of the graph to be equal to the microstrain (ε) and the intercept on the $\beta\cos\theta$ axis equals to $\frac{0.9\lambda}{D}$. Therefore, the crystallite size is given as

$$D = \frac{0.9\lambda}{inteecept\ on\ \beta\ \cos\theta\ axis} \tag{13}$$

Figure 12 shows the Williamson-Hall (W-H) plot of CdSe/ZnSe thin films annealed at 523 K. From the figure, the crystallite size of the CdSe/ZnSe superlattice thin film annealed at 523K was found to be 5.546 nm while dislocation density and microstrain values obtained were 3.25×10^{16} lines/m^2 and 1.13×10^{-2} respectively. The negative slope observed in the W-H plot of Figure 12 could be a result of lattice shrinkage due to compressive strain that occurred due to annealing which also is evidence of formation of improved crystalline CdSe/ZnSe thin film at 523 K [54-55].

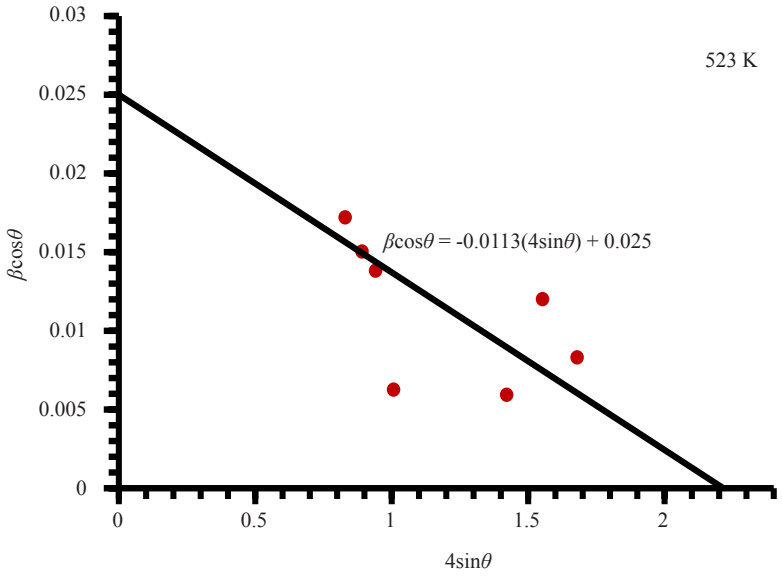

Figure 12. W-H plot for cadmium selenide/zinc selenide (CdSe/ZnSe) thin films annealed at 523 K

3.5 *Morphological properties*

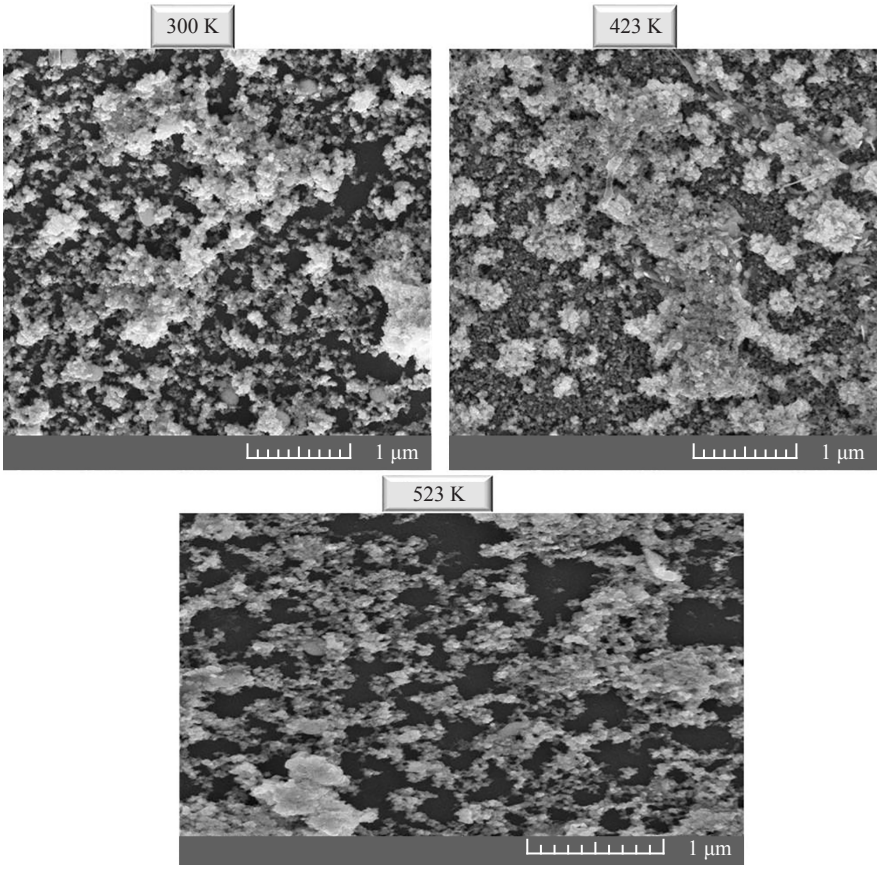

Figure 13. SEM images of SILAR deposited CdSe/ZnSe superlattice thin films at 300 K, annealed at 423 K and 523 K

Figure 13 showed SEM images of as-deposited CdSe/ZnSe superlattice thin film and those annealed at 423 K and 523 K. SEM image of as-deposited CdSe/ZnSe superlattice thin film revealed the formation of agglomerated tiny nanoparticles of different dimensions and sizes. SEM images of CdSe/ZnSe film annealed at 432 K and 523 K revealed that the surface of superlattice thin film contained agglomerated mass of nanoparticles of different sizes and shapes.

4. Conclusion

The analysis of the results of the characterizations done on the CdSe/ZnSe superlattice thin films to determine the effects of annealing temperatures on their properties showed that the optical properties such as absorbance, reflectance, refractive index and extinction coefficient of the films which were low are improved as a result of increase in the annealing temperature. The transmittance of the films was found to be high and increased with an increase in wavelength but decreases as the annealing temperature increased. The bandgap energy of the films was also found to be wide but decreased with an increase in the annealing temperature in the range of 2.5 eV to 1.9 eV. The film thickness of the deposited CdSe/ZnSe increased from 136.612 nm to 220.787 nm as the annealing temperature increased. The result of elemental composition via EDS analysis showed that Cadmium (Cd), Zinc (Zn), selenium (Se) and other trace elements such as carbon (C), oxygen (O), sodium (Na) etc. were present in the sample with a light decrease in atomic percentages of cadmium and selenium observed to increase as annealing temperature increased. The XRD results showed that diffraction spectra of the films increase in intensity at annealing temperature of 523 K and the result showed that the deposited thin films are polycrystalline in nature. The crystal parameters such as crystallite size, dislocation density and microstrain of the film at 523 K were found to be 55.46 nm, 3.25×10^{14} l/m^2 and 1.13×10^{-2}. SEM results showed that the CdSe/ZnSe superlattice films formed agglomerated tiny nanoparticles of different dimensions and sizes which increased as annealing temperature increased from 432 K to 523 K. These results showed that the deposited superlattice thin films of CdSe/ZnSe can be used for many optoelectronic applications like photovoltaic cell, LEDs etc. regarding the position of their bandgap energy and other properties.

Acknowledgement

The authors which to acknowledge the staff of Nanotech Research Laboratory, Department of Physics and Astronomy, University of Nigeria Nsukka, Enugu State, Nigeria for availing their laboratory for us to carry out the optical analysis of the samples. The team of scientists of Material Research Department, iThemba Labs, Johannesburg, South Africa, and Electronic Microscope Unit, University of Cape Town, also in South Africa are also acknowledged for painstakingly handling and carrying out the structural, compositional as well as the morphological analysis of the samples in their respective laboratories in South Africa.

Conflicts of interest

The authors declare that there was no conflict of any interest that occurred during and after this research work.

References

[1] Hussain S, Iqbal M, Khan AA, Khan MN, Mehboob G, Ajmal S, et al. Fabrication of nanostructured cadmium selenide thin films for optoelectronics applications. *Frontier in Chemistry*. 2021; 9(661723): 1-12. Available from: https://doi.org/10.3389/fchem.2021.661723.

[2] Hasaneen MF, Alrowaili ZA, Mohamed WS. Structure and optical properties of polycrystalline ZnSe thin films: validity of Swanepol's approach for calculating the optical parameters. *Material Research Express*. 2020; 7(016422): 1-15. Available from: https://doi.org/10.1088/2053-1591/ab6779.

[3] Chowdhury MT, Zubair MA, Takeda H, Hussain KMA, Islam MF. Optical and structural characterization of ZnSe

thin film fabricated by thermal vapour deposition technique. *AIMS Materials Science*. 2017; 4(5): 1095-1121. Available from: https://doi.org/10.3934/matersci.2017.5.1095.
[4] Guzeldir B, Saglam M, Ates A. Effects of SILAR cycle on the electrical characteristics of Cd/CdSe/n-Si/Au-Sb structure. *Turkish Journal of Physics*. 2011; 35: 1-12.
[5] Debele T, Gashaw F. Effect of temperature on morphological, structural and optical properties of cadmium selenide (CdSe) thin films deposited by chemical bath deposition method. *Advances in Life Science and Technology*. 2018; 67: 12-16.
[6] Rosly HN, Rahman KS, Abdullah SF, Harif MN, Doroody C, Chelvanathan P, et al. The role of deposition temperature in the photovoltaic properties of RF-sputtered CdSe thin films. *Crystals*. 2021; 1(11): 1-13. Available from: https://doi.org/10.3390/cryst11010073.
[7] Kumara P, Kumar D, Kumar A, Katiyar KS. Effect of post growth annealing process on optical properties of CdSe thin films on Si p-type substrate deposited by pulsed laser deposition technique. *The International Journal of Analytical and Experimental Modal Analysis*. 2021; 13(6): 3016-3028.
[8] Khairnar U, Behere S, Pawar P. Optical properties of polycrystalline zinc selenide thin films. *Materials Sciences and Applications*. 2012; 3(1): 36-40. Available from: http://dx.doi.org/10.4236/msa.2012.31006.
[9] Lalhriatzuala, Agarwal P. Preparation and characterization of Znse thin film for photovoltaic applications. *International Journal Of Innovative Research & Development*. 2012; 1(12): 104-110.
[10] Sharma J, Shikha D, Tripathi SK. Electrical characterization of nanocrystalline zinc selenide thin films. *Journal of Theoretical and Applied Physics*. 2012; 6(16): 1-5. Available from: http://www.jtaphys.com/content/6/1/16.
[11] Qasrawi AF, Taleb MF. Enhancement of electrical performance of ZnSe thin films via Au nanosandwiching. *Materials Science-Poland*. 2020; 38(1): 174-180. Available from: http://www.materialsscience.pwr.wroc.pl/.
[12] Lakshmikandhan T. Synthesis of ZnSe thin film by chemical bath deposition and for photovoltaic application. *Malaya Journal of Matematik*. 2020; S(2): 2237-2239. Available from: https://doi.org/10.26637/MJM0S20/0575.
[13] Chaudhari KB, Gosavi NM, Deshpande NG, Gosavi, SR. Chemical synthesis and characterization of CdSe thin films deposited by SILAR technique for optoelectronic applications. *Journal of Science Advanced Materials and Devices*. 2016; 1: 476-481. Available from: https://doi.org/10.1016/j.jsamd.2016.11.001.
[14] Ikhioya IL, Ekpunobi AJ. The optical properties of CdSe/ZnSe superlattice by electrodeposition technique. *Journal of the Nigerian Association of Mathematical Physics*. 2014; 28(2): 289-296.
[15] Bashar MS, Yusoff Y, Abdullah SF, Rahaman M, Chelvanathan P, Gafur A, et al. An investigation on structural and optical properties of $Zn_{1-x}Mg_xS$ thin films deposited by RF magnetron Co-sputtering technique. *Coatings*. 2020; 10(766): 1-13. Available from: https://doi.org/10.3390/coatings10080766.
[16] Nwamaka IA, Asiegbu AD, Nnanna LA, Ikhioya IL. Investigation on the influence of varying substrate temperature on the physical features of yttrium doped cadmium selenide thin films materials. *SSRG International Journal of Applied Physics*. 2021; 8(2): 37-46. Available from: https://doi.org/10.14445/23500301/IJAP-V8I2P106.
[17] Deng YL, Xu ZY, Cai K, Ma F, Hou J, Peng SL. The effect of Mn-doped ZnSe passivation layer on the performance of CdS/CdSe quantum dot-sensitized solar cells. *Chinese Physics B*. 2019; 28(9): 098802. Available from: https://doi.org/10.1088/1674-1056/ab37f3.
[18] Shinde SK, Dubal DP, Ghodake GS, Fulari VJ. Electronic impurities (Fe, Mn) doping in CdSe nanostructures for improvements in photoelectrochemical applications. *RSC Advances*. 2014; 4(63): 33184-33189. Available from: https://doi.org/10.1039/C4RA02791D.
[19] Deng Z, Lie FL, Shen S, Ghosh I, Mansuripur M, Muscat AJ. Water-based route to ligand-selective synthesis of ZnSe and Cd-doped ZnSe quantum dots with tunable ultraviolet A to blue photoluminesce. *Langmuir*. 2009; 25(1): 434-442.
[20] Solanki R, Huo J, Freeouf JL, Miner B. Atomic layer deposition of ZnSe/CdSe superlattice nanowires. *Applied Physics Letters*. 2002; 81(20): 3864-3866. Available from: https://doi.org/10.1063/1.1521570.
[21] Nwori AN, Ezenwaka LN, Ottih IE, Okereke NA, Umeokwona SN, Okoli NL, et al. Study of the optical and solid-state properties of copper manganese sulphide (CuMnS) thin film semiconductors for possible optoelectronics applications. *Journal of Physics and Chemistry of Materials*. 2021; 8(3): 23-33.
[22] Ijeh RO, Nwanya AC, Nkele AC, Madiba IG, Khumalo Z, Bashir AKH, et al. Magnetic and optical properties of electrodeposited nanospherical copper doped nickel oxide thin films. *Physica E: Low-dimensional Systems and Nanostructures*. 2019; 113: 233-239. Available from: https://doi.org/10.1016/j.physe.2019.05.013.
[23] Shinen MH, Alsaati SAA, Rasooqi FZ. Preparation of high transmittance TiO_2 thin films by sol gel techniques as antireflection coating. *Journal of Physics, Conference Series*. 2018; 1032: 1-11. Available from: http://dx.doi.org/10.1088/1742-6596/1032/1/012018.
[24] Al-Dahaan SAJ, Al-khayatt AHO, Salman MK. The optical properties of Fe_2O_3 thin film prepared by chemical

spray pyrolysis deposition (CSP). *Journal of Kufa-Physics*. 2014; 6(2): 16-23.
[25] Guneri E, Kariper A. Characterization of high quality chalcogenide thin films fabricated by chemical bath deposition. *Electronic Materials Letters*. 2013; 9(1): 13-17. Available from: https://doi.org/10.1007/s13391-012-2099-6.
[26] Augustine C, Nnabuchi MN, Chikwenze RA, Anyaegbunam FNC, Kalu PN, Robert BJ, et al. Comparative investigation of some selected properties of Mn_3O_4/PbS and CuO/PbS composites thin films. *Material Research Express*. 2019; 6: 1-10.
[27] Kariper IA. Synthesis and characterization of CrSe thin film produced via chemical bath deposition. *Optical Review*. 2017; 24(2): 139-146. Available from: https://doi.org/10.1007/s10043-017-0307-1.
[28] Kariper IA. A new route to synthesis MnSe thin films by chemical bath method. *Material Research*. 2018; 21(2): 1-6. Available from: http://dx.doi.org/10.1590/1980-5373-MR-2017-0215.
[29] Ongwen NO, Oduor AO, Ayieta EO. Effect of concentration of reactants on the optical properties of iron-doped cadmium stannate thin films deposited by spray pyrolysis. *American Journal of Materials Science*. 2019; 9(1): 1-7. Available from: https://doi.org/10.5923/j.materials.20190901.01.
[30] Sreedev P, Rakhesh V, Roshina NS. Optical characterization of ZnO thin films prepared by chemical bath deposition method. *IOP Conf. Series: Materials Science and Engineering*. 2018; 377(012086): 1-7. Available from: http://dx.doi.org/10.1088/1757-899X/377/1/012086.
[31] Tauc J, Grigorovici R, Vancu A. Optical properties and electronic structure of amorphous germanium. *Physics Status Solid*. 1966; 15(2): 627-637. Available from: https://doi.org/10.1002/pssb.19660150224.
[32] Tezel FM, Ozdemir O, Kariper IA. The effects of pH on structural and optical characterization of iron oxide thin films. *Surface Review and Letters*. 2017; 24(4): 1-10. Available from: https://doi.org/10.1142/S0218625X17500512.
[33] Kannan S, Subiramaniyam NP, Sathishkumar M. Effect of annealing temperature and Mn doping on the structural and optical properties of ZnS thin films for enhanced photocatalytic degradation under visible light irradiation. *Inorganic Chemistry Communications*. 2020; 119: 108068. Available from: https://doi.org/10.1016/j.inoche.2020.108068.
[34] Hojamberdiev M, Piccirillo C, Cai Y, Kadirova ZC. ZnS-containing industrial waste: Antibacterial activity and effects of thermal treatment temperature and atmosphere on photocatalytic activity. *Journal of Alloys and Compounds*. 2019; 791: 971-982. Available from: https://doi.org/10.1016/j.jallcom.2019.03.368.
[35] Kabir MH, Ali MM, Kaiyum MA, Rahman MS. Effect of annealing temperature on structural morphological and optical properties of spray pyrolized Al-doped ZnO thin films. *Journal of Physics Communications*. 2019; 3(10): 1-11. Available from: https://doi.org/10.1088/2399-6528/ab496f.
[36] Rani S, Shanthi J, Kashif M, Ayeshamariam A, Jayachandran M. Studies on different doped Zn concentrations of CdSe thin films. *Journal of Powder Metallurgy & Mining*. 2016; 5(143): 1-7. Available from: https://doi.org/10.4172/2168-9806.1000143.
[37] Gode F, Kariper IA, Guneri E, Unlu S. Effect of complexing agents on the structural, optical and electrical properties of polycrystalline indium sulphide thin films deposited by chemical bath method. *Acta Physica Polonica A*. 2017; 132(3): 527-530. Available from: http://doi.org/10.12693/APhysPolA.132.527.
[38] Gode F, Unlu S. Nickel doping effect on the structural and optical properties of indium sulfide thin films by SILAR. *Open Chemistry*. 2018; 16: 757-762. Available from: http://dx.doi.org/10.1515/chem-2018-0089.
[39] Chaudhary P, Kumar V. Preparation of ZnO thin film using sol-gel dip-coating technique and their characterization for optoelectronic applications. World Scientific News. 2019; 121: 64-71. Available from: http://www.worldscientificnews.com.
[40] Ezenwaka LN, Okoli NL, Okereke NA, Ezenwa IA, Nwori AN. Properties of electrosynthesized cobalt doped zinc selenide thin films deposited at varying time. *Nanoarchitectonic*. 2022; 3(1): 1-17. Available from: http://ojs.wiserpub.com/index.php/NAT/.
[41] Bakri AS, Sahdan MZ, Adriyanto F, Raship NA, Said NDM, Abdullah SA, et al. Effect of annealing temperature of titanium dioxide thin films on structural and electrical properties. *AIP Conference Proceedings*. 2017; 1788(1): 1-8. Available from: https://doi.org/10.1063/1.4968283.
[42] Kavitha M, Saroja M, Jenifer G. The annealing effect of zinc selenide thin film using CBD technique for PV solar cell application. *International Journal of Materials Science and Engineering*. 2017; 5(3): 110-115.
[43] Egwunyenga NJ, Okoli NL, Nwankwo IE, Obimma IO. Effect of annealing temperature on optical and structural properties of EDTA mediated solution grown zinc selenide thin films. *Energy Research*. 2020; 4(3): 21-33.
[44] Lee SM, Joo YH, Kim CI. Influences of film thickness and annealing temperature on properties of sol-gel derived ZnO-SnO_2 nanocomposite thin film. *Applied Surface Science*. 2014; 320: 494-501. Available from: https://doi.org/10.1016/j.apsusc.2014.09.099.

[45] Geethanjali PM, Deepa K, Remadevi TL. Effect of number of cycles on SILAR deposited ZnSe thin films. *AIP Conference Proceedings*. 2021; 2352(1): 1-5. Available from: https://doi.org/10.1063/5.0052381.
[46] Lesnyak V, George C, Genovese A, Prato M, Casu A, Ayyappan S, et al. Alloyed copper chalcogenide nanoplatelets via partial cation exchange reactions. *ACS Nano*. 2014; 8(8): 8407-8418. Available from: https://doi.org/10.1021/nn502906z.
[47] Khan M, Mishra A, Shukla J, Sharma P. X-ray analysis of $BaTiO_3$ ceramics by Williamson-Hall and size strain plot methods. *AIP Conference Proceedings*. 2019; 2100(1): 1-4. Available from: https://doi.org/10.1063/1.5098692.
[48] Ghasemi HM, Zamanian M, Souri D. Williamson-Hall analysis in evaluation of lattice strain and the density of lattice dislocation for nanometer scaled ZnSe and ZnSe:Cu particles. *Ceramics International*. 2019; 45(11): 14084-14089. Available from: https://doi.org/10.1016/j.ceramint.2019.04.107.
[49] Hassanien AS, Neffati R, Aly KA. Impact of Cd-addition upon optical properties and dispersion parameters of thermally evaporated CdxZn1-xSe films: Discussions on bandgap engineering, conduction and valence band positions. *Optik-International Journal for Light and Electron Optics*. 2020; 212(164681): 1-20. Available from: https://doi.org/10.1016/j.ijleo.2020.164681.
[50] Prablu YT, Rao KV, Kumar VSS, Kumari BS. X-ray Analysis by Williamson-Hall and Size-Strain plot methods of ZnO nanoparticles with fuel variation. *World Journal of Nano Science and Engineering.* 2014; 4: 21-28. Available from: https://doi.org/10.4236/wjnse.2014.41004.
[51] Narayana STN, Pushpalatha HL, Ganesha R. Synthesis of CdSe thin film by chemical bath deposition and characterization. *International Journal of Engineering Science and Innovative Technology (IJESIT)*. 2017; 6(1): 41-49.
[52] Ezenwaka LN, Nwori AN, Otti IE Okereke NA, Okoli NL. Investigation of the optical, structural and compositional properties of electrodeposited lead manganese sulfide (PbMnS) thin films for possible device applications. *Nanoarchitectonic.* 2022; (1): 18-32. Available from: https://doi.org/10.37256/nat.3120221226.
[53] Egwunyenga NJ, Ezenwaka LN, Ezenwa IA, Okoli NL. Effect of annealing temperature on the optical properties of electrodeposited ZnO/MgO superlattice. *Materials Research Express*. 2019; 6(10): 1-9. Available from: https://doi.org/10.1088/2053-1591/ab42ab.
[54] Dey P, Sarkar S, Das R. X-ray diffraction study of the elastic properties of jagged spherical CdS nanocrystals. *Materials Science-Poland*. 2020; 38(2): 271-278. Available from: https://doi.org/10.2478/msp-2020-0032.
[55] Murugesan C, Chandrasekaran G. Impact of Gd^{3+} substitution on the structural, magnetic and electrical properties of cobalt ferrite nanoparticles. *RSC Advances*. 2015; 5(90): 73714-73725. Available from: https://doi.org/10.1039/C5RA14351A.